Materials Advances

ROYAL SOCIETY OF CHEMISTRY

PAPER

View Article Online
View Journal | View Issue

Cite this: *Mater. Adv.*, 2026, 7, 2268

Green synthesis of a CQD/AGNPS composite from guava leaf and its potent antimicrobial activity against multidrug-resistant ESKAPEE pathogens

Hoang Thi Thu, *[a] Le Tuan Anh,[b] Dang Thien Huong[c] and Duong Ngoc Huyen[a]

Received 24th July 2025,
Accepted 7th January 2026

DOI: 10.1039/d5ma00802f

rsc.li/materials-advances

This study presents a green synthesis approach for fabricating CQD/AgNPs nanocomposite materials, in which carbon quantum dots (CQDs) were derived from dried guava leaves (*Psidium guajava*)—a widely available, low-cost, and accessible plant material in Vietnam. The resulting nanocomposite was characterized using a range of advanced techniques, including UV-Vis, PL, XRD, FTIR, Raman, SEM and TEM. These analyses confirmed the formation of uniformly dispersed, spherical nanoparticles with an average diameter of approximately 33.4 nm and good structural stability. Interestingly, the CQD/AgNPs nanocomposite demonstrated strong antibacterial activity against multidrug-resistant (MDR) pathogens of the ESKAPEE group. In particular, the material exhibited a minimum inhibitory concentration (MIC) of 25 μg mL^{-1} towards *Acinetobacter baumannii*, a highly drug-resistant bacterium commonly associated with hospital-acquired infections. The nanocomposite also showed significant inhibitory effects against ciprofloxacin-resistant strains of *Staphylococcus aureus*, *Klebsiella pneumoniae*, *Pseudomonas aeruginosa*, and *Enterobacter* spp., with MIC values of 50 μg mL^{-1}. This report is among the first to develop a green-synthesized CQD/AgNP nanomaterial with low production cost, good industrial scalability, and long-term stability at room temperature. Additionally, the study also comprehensively evaluates the material's antibacterial activity against five drug-resistant ESKAPEE pathogens, thereby highlighting its potential application as an alternative to conventional antibiotics.

1. Introduction

The global rise in infections caused by multidrug-resistant (MDR) pathogens, particularly the ESKAPEE group (*Enterococcus faecium*, *Staphylococcus aureus*, *Klebsiella pneumoniae*, *Acinetobacter baumannii*, *Pseudomonas aeruginosa*, *Enterobacter* spp., and *Escherichia coli*), poses a significant threat to public health systems worldwide.[1,2] The widespread misuse and overuse of antibiotics in both clinical and agricultural settings have accelerated the evolution of resistance mechanisms, thereby diminishing the efficacy of conventional antimicrobial therapies.[3] In the European Union and European Economic Area (EU/EEA), antimicrobial-resistant infections are estimated to cause over 35 000 deaths annually—a number that continues to rise each year.[4] Among the ESKAPEE group, *Klebsiella pneumoniae* and *Acinetobacter baumannii* have raised major concerns. According to the 2023 EARS-Net report, the incidence of bloodstream infections caused by carbapenem-resistant *K. pneumoniae* in the European Union reached 3.97 cases per 100 000 population, increasing 57.5 percent compared to 2019. Notably, infections caused by carbapenem-resistant *A. baumannii* rose by over 121% between 2018 and 2021, with the majority of isolates also exhibiting resistance to fluoroquinolones and aminoglycosides (ECDC, 2023). These findings highlight the growing threat of extensively drug-resistant bacteria and emphasize the urgent need for new, effective, and sustainable antibacterial strategies.[5–7]

Nanotechnology, particularly the use of silver nanoparticles (AgNPs), has attracted considerable attention in the search for alternative antimicrobial solutions.[8,9] AgNPs exhibit broad-spectrum activity and act through multiple mechanisms, demonstrating strong efficacy against both Gram-positive and Gram-negative bacteria.[8,10,11] However, conventional synthesis methods often rely on toxic reducing agents such as sodium borohydride, sodium hydroxide, hydrochloric acid or hydrazine, raising concerns regarding environmental safety, biocompatibility, and feasibility for practical applications.

To overcome these limitations, green synthesis approaches have emerged as a promising alternative. By employing plant extracts, polysaccharides, or natural polymers as both reducing and stabilizing agents, these methods offer a more sustainable and environmentally friendly route for the production of

[a] *Faculty of Fundamental Science, Industrial University of Ho Chi Minh City, Ho Chi Minh City, Vietnam. E-mail: hoangthithu@iuh.edu.vn, hoangthukhcn@gmail.com; Tel: +84986062980*
[b] *School of Pharmacy, University of Medicine and Pharmacy at Ho Chi Minh city, Vietnam*
[c] *Lawrence S. Ting School, 1 Raymondienne Street, Tan My Ward, Ho Chi Minh City, Vietnam*

AgNPs.[12–17] Numerous studies have reported the strong antimicrobial performance of biosynthesized AgNPs, reinforcing their potential for biomedical and environmental applications. For instance, the study by Trieu *et al.* (2025)[18] demonstrated that AgNPs synthesized using *Psidium guajava* (guava) leaf extract exhibited potent antibacterial activity against both Gram-positive (*Staphylococcus aureus*, *Enterococcus faecalis*) and Gram-negative (*Pseudomonas aeruginosa*) species. Similarly, Chartarrayawadee *et al.* (2020) synthesized AgNPs *via* a green route using an extract from *Lysimachia foenum-graecum* Hance. The resulting nanoparticles showed prolonged colloidal stability and strong antibacterial activity against *S. aureus*, with an inhibition zone diameter of 19.08 ± 0.67 mm—exceeding that of the positive control, chloramphenicol.[13] More recently, Raza *et al.* (2023) developed "TeaNPs" using three types of tea infusions (black, green, and red) and found that green tea-derived nanoparticles (GTeaNPs) were the most active, eliminating up to 80% of Gram-negative bacterial cells within 3 h at 100 μg mL^{-1}—significantly outperforming ampicillin under the same conditions.[18]

Although green-synthesized AgNPs have demonstrated strong and broad-spectrum antibacterial activity, certain drawbacks remain, including the need for refrigerated storage (≈ 4 °C) and relatively high MIC values, which hinder practical application. Recently, combining AgNPs with carbon quantum dots (CQDs) has gained attention as an effective strategy to enhance antibacterial efficiency while maintaining environmental safety. CQDs can act as both reducing and stabilizing agents during AgNP formation and improve bacterial adhesion, thereby enhancing antibacterial efficacy through a synergistic mechanism.[19–21]

Carbon quantum dots (CQDs) are a class of carbon-based nanomaterials known for their environmental friendliness, high photostability, and strong electron-transfer capability.[22–25] They can be readily synthesized from a wide range of biomass sources, including leaves, fruit peels, and agricultural residues.[26] Common synthetic routes include hydrothermal treatment, microwave-assisted processes, and high-temperature carbonization.[23,27–30] These methods offer low cost, operational simplicity, and good scalability.[24,26] CQDs also exhibit mild antibacterial activity due to the reactive surface functional groups.[31] In addition, they provide slight wound-healing support, which is associated with their antioxidant properties and high biocompatibility.[19,32,33]

In this study, we report the fabrication of a CQD/AgNPs nanocomposite using an environmentally friendly physical approach that yields a stable product at room temperature and is suitable for large-scale production. Furthermore, the antibacterial activity of the synthesized nanocomposite was comprehensively evaluated against clinically relevant multidrug-resistant (MDR) ESKAPEE pathogens, providing valuable insights for the practical development of eco-friendly antimicrobial agents.

2. Materials and methods

2.1. Materials

Guava leaves were collected and dried. Polyvinyl alcohol PVA-124 (China) and silver nitrate ($AgNO_3$, Prolabo – France) were used in the synthesis. Dialysis tubing with a cut-off of 2000 Da was purchased from Spectrum Lab (USA).

For antibacterial testing, nutrient broth (NB) and nutrient agar (NA) were purchased from Oxoid Ltd (Basingstoke, Hampshire, UK).

The multidrug-resistant (MDR) bacterial strains used in this study included *Acinetobacter baumannii* VS73, *Escherichia coli* ND01, methicillin-resistant *Staphylococcus aureus* (MRSA) VS02, *Klebsiella pneumoniae* VS39, and *Pseudomonas aeruginosa* ND26. These strains were isolated from clinical samples by the Department of Microbiology–Parasitology, Faculty of Pharmacy, University of Medicine and Pharmacy at Ho Chi Minh City, Vietnam.

All strains were stored in glycerol at −80 °C. Before testing, they were revived by streaking onto Mueller–Hinton agar plates and incubated overnight at 37 °C. Then, 2–3 colonies of each strain were picked and suspended in PBS until the optical density at 600 nm reached 0.08–0.1, equivalent to about 10^8 CFU mL^{-1}. This bacterial suspension was further diluted with PBS to around 10^6 CFU mL^{-1} and used within 15 minutes after preparation.

Ciprofloxacin disks were obtained from Bio Techem Co., LTD (Vietnam). Other available chemicals were purchased from El-Gomhouria for Trading Chemicals and Medical Appliances (Alexandria, Egypt) and used without further purification.

2.2. Carbon quantum dots (CQDs-G) synthesis

Three grams of dried guava leaves were added to a 200 mL stainless steel cup and carbonized at 800 °C in a muffle furnace. After 15 minutes, the sample was rapidly cooled by removing it from the furnace and pouring in 50 mL of distilled water. The mixture was then poured into an autoclave, the lid was sealed tightly, and the autoclave was placed in a furnace. The furnace was set to 400 °C and heated for 10 h. After that, we waited for the furnace to cool completely to room temperature before proceeding. The mixture was stirred with a magnetic stirrer for 30 minutes, microwaved for 5 minutes, and then left to settle for 2 days. It was roughly filtered through 47 μm filter paper, then transferred to a dialysis bag (molecular weight cutoff: 2000 Da) and dialyzed in distilled water for 3 days. The final solution was gently heated at 70 °C until the volume was roughly 20 mL, and was then used to synthesize the CQD/AgNPs nanocomposite.

2.3. CQD/AgNPs nanocomposite synthesis

2.3.1. Preparation of the CQD/AgNPs nanocomposite. The green synthesis process of CQD/AgNPs is illustrated in Fig. 1, and began with the dilution of 5 mL of the previously prepared CQD solution being diluted with 420 mL of distilled water, resulting in a total volume of 425 mL. At the same time, 0.835 g of silver nitrate ($AgNO_3$) was dissolved in 25 mL of distilled water to obtain a 0.01 mol solution. Consequently, this $AgNO_3$ solution was added dropwise to the CQDs solution under constant magnetic stirring. The mixture was then adjusted to a final volume of 500 mL with distilled water and stirred at room temperature for 1 hour to promote the interaction between Ag^+ ions and the CQDs.

Meanwhile, 1 g of polyvinyl alcohol (PVA) was dissolved in 500 mL of distilled water under magnetic stirring at room

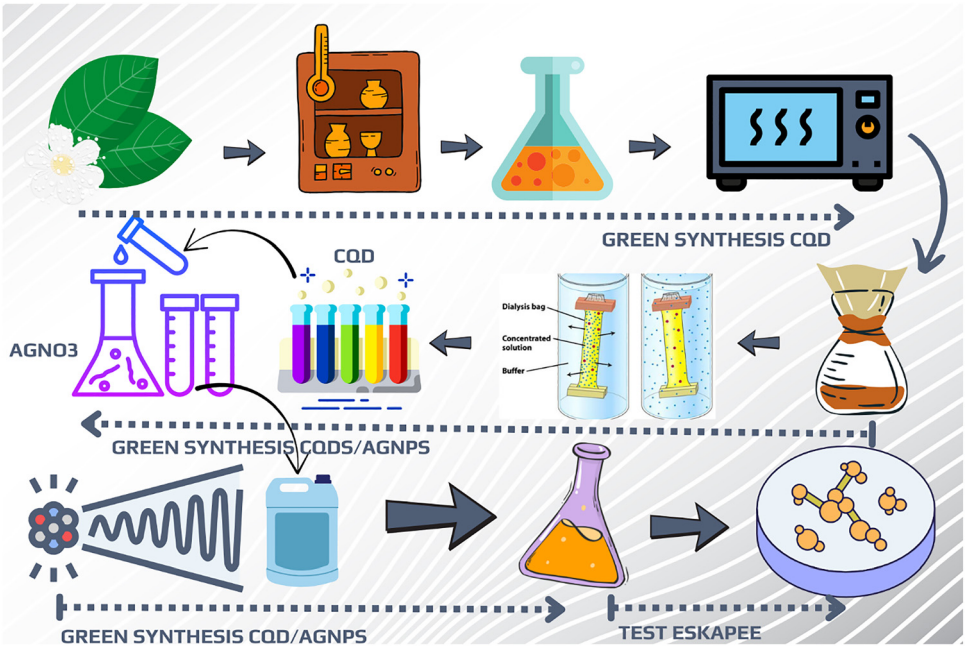

Fig. 1 Green synthesis process of the CQD/AgNPs nanocomposite.

temperature to obtain a homogeneous 0.2% (w/v) PVA solution. The $AgNO_3$/CQDs mixture (500 mL) was then added to the PVA solution while maintaining stirring. The final mixture (1000 mL) was stirred for an additional hour to ensure uniform dispersion of silver ions and CQDs in the PVA matrix.

Eventually, the solution was transferred to PET containers and exposed to gamma irradiation at 25 kGy using a Co-60 source (referred to as sample M1). Gamma irradiation facilitates the *in situ* formation and even distribution of AgNPs and CQDs while embedding them within the PVA network, helping to reduce aggregation. This approach does not require chemical reducing agents or surfactants, aiming for a greener and more efficient synthesis of stable CQD/AgNPs nanocomposites.

2.3.2. Material characterization and instrumentation. The UV-Vis absorption spectra of the samples in aqueous solution were recorded using a Jasco V530 UV-Vis spectrophotometer. The morphology and crystal structure were characterized by scanning electron microscopy (SEM, HITACHI SU8100), transmission electron microscopy (TEM, JEOL JEM-1400), and X-ray diffraction (XRD, D8 ADVANCE with CuKα radiation, λ = 1.54 Å), respectively. Fourier-transform infrared (FT-IR) spectra were obtained using an Equinox 55 FT-IR spectrometer.

2.3.3. Antibacterial activity assay. The antibacterial activity of the CQD/AgNP nanocomposite was evaluated using the agar well diffusion method. Multidrug-resistant (MDR) strains from the ESKAPEE group, including *Acinetobacter baumannii* VS73, *Escherichia coli* ND01, *Staphylococcus aureus* (MRSA) VS02, *Klebsiella pneumoniae* VS39, and *Pseudomonas aeruginosa* ND26, were selected for testing. Bacterial suspensions were prepared as previously described and uniformly spread over Mueller–Hinton agar (MHA) plates using sterile cotton swabs to ensure even distribution.

Sterile wells with a diameter of 6 mm were aseptically punched into the agar plates, and 50 μL of the test sample was added to each well. The plates were then incubated at 37 °C for 18–24 hours to allow the sample to diffuse and interact with bacterial cells in the surrounding agar medium. After incubation, antibacterial activity was determined by measuring the diameter (in mm) of the inhibition zones around the wells, indicating the area where bacterial growth was suppressed. A ciprofloxacin disc (30 μg) was used as a positive control to compare the antimicrobial efficacy with that of a clinically used antibiotic, while sterile distilled water served as a negative control to verify the accuracy of the experimental setup.

2.3.4. Minimum inhibitory concentration (MIC) evaluation. The minimum inhibitory concentration (MIC) of the CQD/AgNPs nanocomposite was determined using the broth microdilution method, following the guidelines of the Clinical and Laboratory Standards Institute (CLSI). The samples were diluted two-fold in Mueller–Hinton Broth (MHB) to create a range of concentrations. Subsequently, 100 μL of each dilution was added to individual wells of a sterile 96-well plate.

Afterward, 5 μL of bacterial suspension ($\sim 10^7$ CFU mL^{-1}) from the MDR strains was added to each well. The plates were then incubated at 37 °C for 24 hours without shaking.

After incubation, the wells were observed directly against a dark background. The MIC was recorded as the lowest concentration where no visible bacterial growth was detected. All tests were performed in triplicate for each strain to ensure consistency and reliability.

2.3.5. Cytotoxicity assay. The cytotoxicity of the synthesized CQD/AgNPs nanocomposite was evaluated using the standard MTT assay on human embryonic kidney (HEK293A) cells to assess its biocompatibility. The cells were cultured in 96-well plates and treated with different concentrations of the nanocomposite (100, 50, 25, 12.5, and 6.25 μg mL^{-1}) for 24 h. After incubation, MTT reagent was added, and the absorbance of the

resulting formazan product was measured at 570 nm using a microplate reader. Cell viability was calculated relative to the untreated control according to standard protocols.

3. Results and discussion

3.1. Characterization of the CQD/AgNPs composite

The UV-Vis absorption spectrum of the CQD/AgNPs composite material (sample M1), as presented in Fig. 2a, exhibits a distinct surface plasmon resonance (SPR) peak at approximately 420 nm. This characteristic peak strongly indicates the formation of silver nanoparticles (AgNPs), as it corresponds to the collective oscillation of conduction electrons on the nanoparticle surface when excited by light. The narrow and symmetrical shape of the SPR band suggests that the synthesized AgNPs are mostly spherical and have a relatively uniform size distribution. The presence of the SPR band confirms the formation of AgNPs, which is consistent with previous studies.[12–14] In addition to the SPR feature, a small shoulder appears in the 300–350 nm region, likely associated with n → π transitions or intrinsic electronic transitions in the carbon core of the carbon quantum dots (CQDs), indicating the coexistence of both CQDs and AgNPs in the nanocomposite. The absence of significant peak broadening or red shift suggests good colloidal stability and minimal aggregation of AgNPs in the presence of CQDs.

To further investigate the optical characteristics of the synthesized CQDs, the photoluminescence (PL) spectra were recorded at different excitation wavelengths (300, 380, and 400 nm), as shown in Fig. 2b. The emission intensity and peak position varied with the excitation wavelength, showing a gradual red-shift from approximately 425 nm to 469 nm as the excitation wavelength increased. This excitation-dependent emission is a typical feature of carbon quantum dots and is generally attributed to multiple emissive surface states and defect-related energy traps. The strong blue emission and relatively short wavelength of the main PL peak suggest that the as-synthesized CQDs possess a small particle size with narrow size distribution. Such behavior reflects the heterogeneous surface structure and confirms the excellent optical tunability of the CQDs, suggesting their strong potential for bioimaging and optoelectronic applications.[22,25,34] However, this estimation is qualitative and based solely on optical observations; the actual particle size and morphology of the CQDs will be further verified by transmission electron microscopy (TEM) analysis.

To examine the crystalline structure of the CQD/AgNPs nanocomposite, X-ray diffraction (XRD) analysis was conducted, as shown in Fig. 3. The diffraction pattern revealed distinct peaks at $2\theta \approx 38.1^\circ$, 44.3°, 64.4°, and 77.4°, corresponding to the (111), (200), (220), and (311) planes of face-centered cubic (fcc) silver, according to JCPDS card no. 04-0783. Using the Debye–Scherrer equation, the average crystallite size of the silver nanoparticles was estimated to be approximately 30 nm. The most intense diffraction peak at 38.1° suggests a preferred orientation along the (111) plane, which is commonly observed in AgNPs synthesized through biological or green methods. The XRD pattern confirms the presence of AgNPs with an fcc structure and indicates good crystallinity and effective particle formation during synthesis, consistent with previous reports on plant-extract-based AgNPs[12,14,20]

In the synthesized sample, no characteristic peaks of silver oxide impurities (Ag_2O, AgO) were observed, indicating that the reduction of Ag^+ ions to metallic Ag^0 was complete.

In addition to the diffraction peaks associated with silver, a broad, low-intensity region was observed around $2\theta \approx 20–25^\circ$. This feature is characteristic of the amorphous structure of carbon quantum dots (CQDs), which has also been reported in previous studies using biomass-derived CQDs.[23,24,27]

Altogether, these results suggest that the CQD/AgNPs nanocomposite consists of highly crystalline silver nanoparticles evenly dispersed within an amorphous carbon background, confirming the successful synthesis of this hybrid material. Moreover, to further assess the particle size and distribution, TEM and SEM analysis of the CQDs and CQD/AgNPs were performed (Fig. 4).

As presented in Fig. 4a, the TEM image indicates that the synthesized CQDs are uniformly dispersed, nearly spherical in shape, and range from 1 to 6 nm in diameter, with an estimated average size of about 4.2 nm.

Furthermore, the SEM image of the CQD/AgNPs (Fig. 4b) nanocomposite reveals well-dispersed, nearly spherical

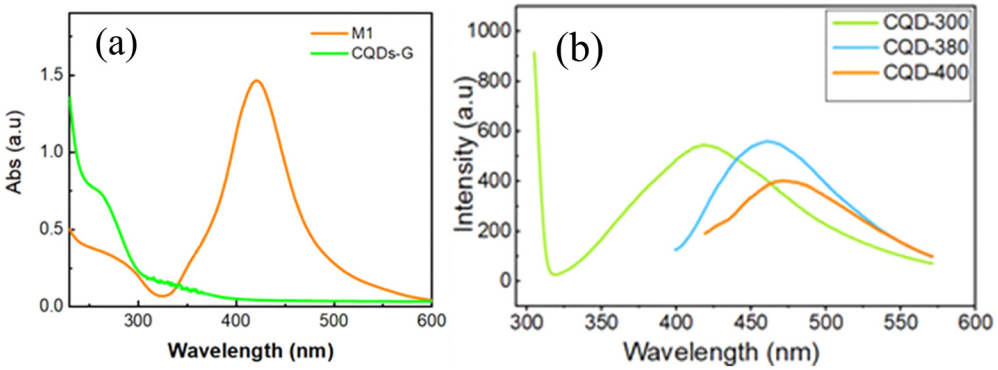

Fig. 2 UV-Vis spectrum of the CQDs (CQDs-G) and CQD/AgNPs nanocomposite (M1) (a). Photoluminescence (PL) spectra of the CQDs recorded under different excitation wavelengths (300, 380, and 400 nm) (b).

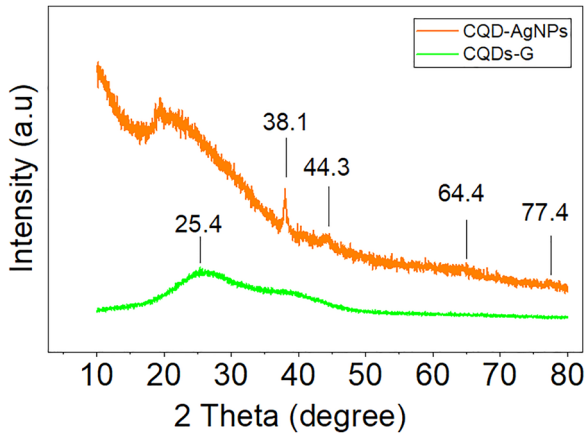

Fig. 3 XRD pattern of CQDs and the CQD/AgNPs nanocomposite (M1) showing crystalline AgNPs peaks and amorphous CQD background.

nanoparticles without noticeable aggregation, suggesting that the CQD matrix effectively prevents agglomeration and contributes to the structural stability of the composite.

In addition, the TEM image and particle size distribution of the CQD/AgNPs nanocomposite (Fig. 4c and d) provide further confirmation, showing uniformly distributed nanoparticles with an average size of approximately 33.4 nm, which is slightly larger than the crystallite size estimated from XRD. This minor discrepancy is likely due to the presence of an amorphous carbon layer encapsulating the Ag nanoparticles, as also reported in several previous studies.[20,35]

Overall, the close correlation among the XRD, SEM, and TEM analyses clearly confirms the successful synthesis of well-crystallized, uniformly dispersed AgNPs stabilized within the CQD framework. Such a homogeneous nanostructure is expected

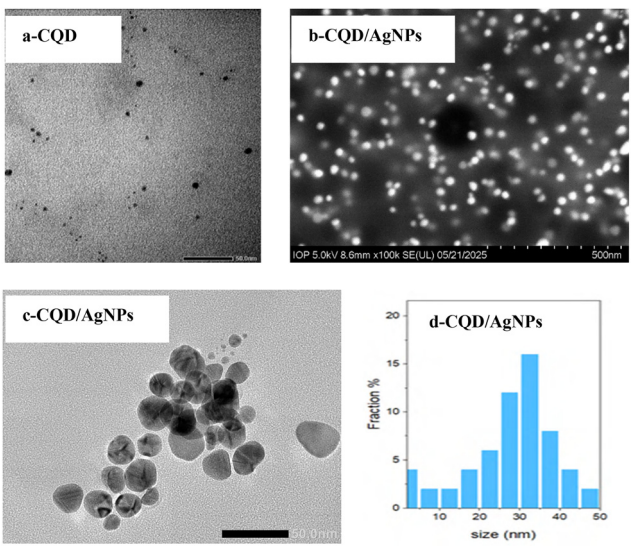

Fig. 4 TEM image of the CQDs-G (scale 50 nm) – (a), SEM image of the CQD/AgNPs nanocomposite (M1) at 500 nm scale showing well-dispersed spherical AgNPs on the carbon quantum dot matrix (b), TEM image of the CQD/AgNPs (scale bar = 50 nm) (c) and particle size distribution of the CQD/AgNPs (d).

to play a crucial role in enhancing the colloidal stability and antimicrobial performance of the CQD/AgNPs composite.

FTIR analysis was conducted to investigate the chemical composition and surface functional groups of the CQD/AgNPs nanocomposite. As shown in Fig. 5, broad absorption bands in the range of 3300–3500 cm^{-1} are attributed to the presence of surface hydroxyl (C–OH) and amine ($–NH_2$) groups. The absorption band observed at approximately 1644 cm^{-1} is assigned to C═C stretching vibrations within aromatic rings. Moreover, the sharp bands at 611 and 720 cm^{-1} correspond to out-of-plane bending vibrations of aromatic C–H bonds. In the CQD/AgNPs nanocomposite, the absorption band at 1644 cm^{-1} is also associated with quinone or conjugated carbonyl (C═O) groups, indicating structural modifications of CQDs during the reduction process. These findings suggest that the coal-derived CQDs possess an aromatic carbon framework with abundant surface amino and phenolic hydroxyl groups, which collectively serve as electron donors for reducing Ag^+ ions into elemental silver (Ag^0).

In addition to their reductive function, these surface functional groups also play a vital role in modulating the antimicrobial behavior of the CQD/AgNPs nanocomposite. The –COOH, –OH, and $–NH^2$ groups enhance the adhesion and electrostatic interaction between the nanocomposite and bacterial cell membranes, improving surface contact and facilitating the release of Ag^+ ions as well as the generation of reactive oxygen species (ROS).[19,20] Such interactions increase membrane permeability and promote the penetration of AgNPs into bacterial cells, ultimately contributing to the enhanced antibacterial activity of the CQDs/AgNPs composite.

The structural characteristics of CQD/AgNPs were further validated through Raman spectroscopic analysis. As illustrated in Fig. 6, the Raman spectrum displays two prominent peaks located at 1320 cm^{-1} and 1580 cm^{-1}, which are attributed to the D and G bands of graphitic carbon, respectively.[36–38] The calculated ID/IG ratio of 1.03 indicates a predominantly amorphous structure with a high degree of disorder. This ratio also reflects the relative abundance of sp^3 to sp^2 hybridized carbon, suggesting the presence of structural imperfections within the green synthesized CQDs. In addition to the characteristic D and

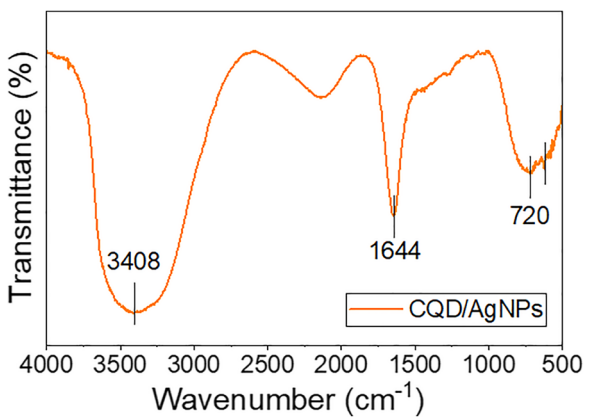

Fig. 5 FTIR of CQD/AgNPs.

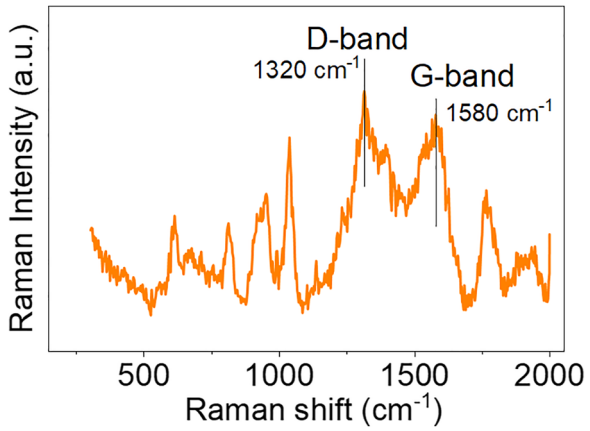

Fig. 6 Raman spectrum of CQD/AgNPs.

G bands, several sharper Raman peaks can be observed in the 1000–1600 cm^{-1} region. These additional peaks may originate from the vibrational modes of organic functional groups such as C–H, C═O, and C–N, which are derived from residual biomolecules of the guava-leaf precursor that remain adsorbed on the nanocomposite surface. Similar Raman features have been reported for biologically synthesized AgNPs that are coated with or interact with polyphenolic compounds.[36,37] The presence of these surface organic species is also consistent with the FTIR results, indicating that these functional groups contribute to improving the dispersion and colloidal stability of the CQDs/AgNPs system in aqueous solutions.

In summary, the structural analyses from Raman spectroscopy, together with SEM, TEM, XRD, UV-Vis, and FTIR measurements, confirm the successful synthesis of a stable and uniform CQD/AgNPs nanocomposite at the nanoscale. The coexistence of crystalline silver phases and amorphous carbon components verifies the hybrid nature of the material. The uniform morphology and nanoscale dimensions provide a high surface-area-to-volume ratio, facilitating effective contact and interaction between the nanocomposite and microbial cells—an important factor contributing to the antibacterial performance discussed in the following section.

3.2. Antibacterial activity

The minimum inhibitory concentration (MIC) values of the CQD/AgNPs nanocomposite against five ESKAPEE bacterial strains are shown in Table 1. These strains—including *Acinetobacter baumannii, Pseudomonas aeruginosa, Klebsiella pneumoniae, Escherichia coli*, and *Staphylococcus aureus*—are well-known clinical pathogens with high resistance to antibiotics, strong biofilm-forming abilities, and frequent association with hospital-acquired infections.

Notably, *A. baumannii* and *P. aeruginosa* are major causes of severe pneumonia and bloodstream infections in intensive care units (ICUs), often resistant to nearly all conventional antibiotics, including carbapenems. *K. pneumoniae* and *E. coli*, though more common, are rapidly acquiring resistance to fluoroquinolones and β-lactams. Meanwhile, *S. aureus*, especially methicillin-resistant strains (MRSA), remains a persistent threat both in community and healthcare settings.

As shown in Table 1, the CQDs/AgNPs nanocomposite exhibited noticeable antibacterial activity, with MIC values ranging from 25 to 50 μg mL^{-1}. In particular, *A. baumannii*—a WHO-prioritized multidrug-resistant pathogen—was completely inhibited at 25 μg mL^{-1}, suggesting a relatively strong antibacterial effect. The other strains (*P. aeruginosa*, *K. pneumoniae*, *E. coli*, and *S. aureus*) were inhibited at 50 μg mL^{-1}, indicating broad-spectrum activity.

For comparison, the MICs of ciprofloxacin against the same strains ranged from 0.5 to 128 μg mL^{-1}, with *A. baumannii* and *K. pneumoniae* showing particularly high resistance (128 μg mL^{-1}). These findings imply that the CQD/AgNPs nanocomposite possesses a promising antibacterial potential, especially toward resistant *A. baumannii*. The enhanced performance may arise from the combined effects of CQDs and AgNPs, which help stabilize the nanoparticles, facilitate Ag^{+} release, and promote ROS generation at the bacterial interface.

To further verify the possible synergistic effect between CQDs and AgNPs, additional comparative antibacterial assays were conducted under identical conditions. The results demonstrated that CQDs alone showed negligible activity (MIC > 1000 μg mL^{-1}), AgNPs alone had an MIC of 50 μg mL^{-1}, whereas the CQDs/AgNPs composite exhibited a markedly enhanced activity with an MIC of 25 μg mL^{-1} against *A. baumannii* as summarized in Table 2. Consistently, the inhibition zone increased from 14 mm (AgNPs) to 17 mm (CQDs/AgNPs). To quantitatively evaluate the interaction between CQDs and AgNPs, the fractional inhibitory concentration (FIC) index was employed as a standard method for determining synergistic effects in antimicrobial combinations. The FIC index is calculated based on the minimum inhibitory concentrations of individual agents and their combinations, providing an objective measure of whether the interaction is synergistic (FIC ≤ 0.5), additive (0.5 < FIC ≤ 1), indifferent (1 < FIC ≤ 4), or antagonistic (FIC > 4).[39]

$$\mathrm{FIC} = \left(\frac{\mathrm{MIC\ A_{combination\ A\&B}}}{\mathrm{MIC_{agent\ A}}}\right) + \left(\frac{\mathrm{MIC\ B_{combination\ A\&B}}}{\mathrm{MIC_{agent\ B}}}\right)$$

Table 1 Minimum inhibitory concentration values of the as-synthesized CQDs and CQD/AgNPs

Sample	MIC (μg mL^{-1}) *Escherichia coli* ND01	MIC (μg mL^{-1}) *Staphylococcus aureus* (MRSA) VS02	MIC (μg mL^{-1}) *Klebsiella pneumoniae* VS39	MIC (μg mL^{-1}) *Acinetobacter baumannii* VS73	MIC (μg mL^{-1}) *Pseudomonas aeruginosa* ND26
CQDs	>1000	>1000	>1000	>1000	>1000
CQD/AgNPs	50	50	50	25	50
Ciprofloxacin	64	128	0.5	128	64

Table 2 Minimum inhibitory concentration and growth inhibition diameter values of the as-synthesized CQDs, AgNPs and CQD/AgNPs

Sample	MIC ($\mu g\ mL^{-1}$)	ZOI (mm)
CQDs	>1000	—
AgNPs	50	14 ± 2
CQD/AgNPs	25	17 ± 2

Table 3 MIC values of the green-synthesized nanomaterials against *Acinetobacter baumannii*

Material	MIC ($\mu g\ mL^{-1}$)	Ref.
AgNPs (Ginkgo)	8	16
CQD/AgNPs (Guava)	25	This study
AgNPs (*Ocimum sanctum* Linn)	32	40
AgNPs	62.5	41
CQD/AgNPs	234	19
AgNPs	125	42
AgNPs (curcumin)	250	17
AgNPs (acroptilon)	50–400	43
Monsonia angustifolia and *Momordica balsamina* Linn extracts	500	44

Applying the standard FIC formula, the calculated value was 0.53, slightly above the conventional synergistic threshold (≤ 0.5). Therefore, this result indicates a near-synergistic interaction, meaning that the presence of CQDs effectively enhances the antibacterial performance of the composite.

Building upon these findings, a comparative overview between our synthesized CQD/AgNPs nanocomposite and other previously reported green-synthesized nanomaterials in terms of antibacterial activity against *Acinetobacter baumannii* is summarized in Table 3.

Table 3 shows that individual plant extracts, such as those from *Psidium guajava* or other medicinal plants, generally exhibit only limited intrinsic antibacterial activity against multidrug-resistant (MDR) bacterial strains, particularly *Acinetobacter baumannii*. Crude plant-based formulations, such as the combination of extracts from *Monsonia angustifolia* and *Momordica balsamina* Linn, require high minimum inhibitory concentrations (MICs), around 500 $\mu g\ mL^{-1}$, to suppress bacterial growth, reflecting their weak inherent antimicrobial potency.[44]

In contrast, when phytochemicals are used as reducing and stabilizing agents during the synthesis of silver nanoparticles (AgNPs), the resulting nanocomposites often show significantly enhanced antibacterial performance. Among reported green-synthesized AgNP systems, the strongest activity was observed in AgNPs derived from *Ginkgo biloba*, with MIC values as low as

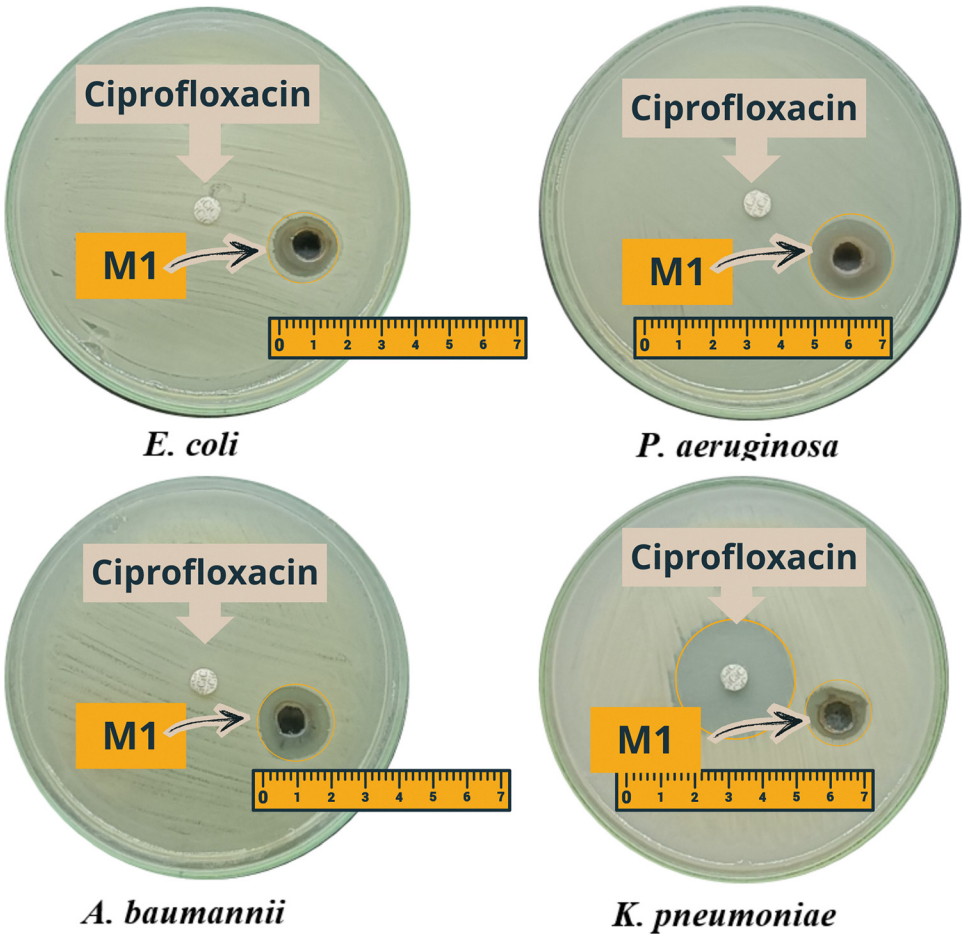

Fig. 7 Images of the inhibition zone of the antibiotic plates and CQD/AgNPs nanocomposite against ESKAPEE pathogens.

8 μg mL^{-1}.[16] Other systems, such as AgNPs synthesized from *Ocimum sanctum* (MIC = 32 μg mL^{-1}),[40] Acroptilon extracts (MIC ranging from 50 to 400 μg mL^{-1})[43] and *Monsonia angustifolia* and *Momordica balsamina* Linn extracts (MIC = 500 μg mL^{-1})[44] also demonstrated improved antibacterial effects although with considerable variability depending on synthesis conditions and particle uniformity.

In our study, the CQD/AgNPs nanocomposite exhibited an MIC of 25 μg mL^{-1} against the carbapenem-resistant *A. baumannii* strain. Although this MIC is slightly higher than that of the most potent Ginkgo-derived AgNPs, it remains within the effective therapeutic range and outperforms many other green-synthesized materials. Notably, our nanocomposite was synthesized *via* a fully green method, free of toxic chemicals. This approach yielded a colloidally stable material that retains functionality over time at room temperature, eliminating the need for refrigerated storage. The combination of long-term room temperature stability, the use of abundant and locally available biomass feedstock, and a synthesis method that is scalable makes our nanocomposite a promising candidate for industrial-scale production.

To visually illustrate the antibacterial efficacy of the CQD/AgNPs nanocomposite (sample M1), we performed zone of inhibition (ZOI) assays against four clinically isolated multidrug-resistant (MDR) bacterial strains, namely *Escherichia coli*, *Klebsiella pneumoniae*, *Acinetobacter baumannii*, and *Pseudomonas aeruginosa*, as shown in Fig. 7. These ESKAPEE group strains were isolated from clinical specimens at the University Medical Center in Ho Chi Minh City (UMC-HCMC) and were confirmed to be resistant to ciprofloxacin as well as several other commonly used antibiotics

As shown in Fig. 7, *E. coli*, *A. baumannii*, and *P. aeruginosa* showed no measurable inhibition zones with ciprofloxacin, confirming their resistance. In contrast, sample M1 displayed clear antibacterial activity, with ZOI diameters of 15 mm, 17 mm, and 17 mm, respectively. For *K. pneumoniae*, ciprofloxacin (30 μg mL^{-1}) still produced a large inhibition zone of 30 mm, while M1 showed a smaller ZOI of about 13 mm. Nevertheless, M1 demonstrated broad-spectrum antibacterial activity across multiple ESKAPEE strains. These findings highlight the potential of the CQD/AgNPs nanocomposite as an alternative antimicrobial agent against multidrug-resistant bacteria, with possible applications as a disinfectant or hand sanitizer for healthcare workers (Table 4).

The remarkable antibacterial activity of the CQD/AgNPs composite can be attributed to the combined contributions of carbon quantum dots and silver nanoparticles. The well-dispersed AgNPs continuously release Ag^+ ions, which interact with bacterial cell walls and intracellular components, leading to membrane disruption and cell death, as illustrated in Fig. 8. Meanwhile, the CQDs provide abundant surface functional groups (–COOH, –OH, –NH_2) that enhance the adhesion of the composite to bacterial membranes, improve dispersion stability, and facilitate reactive oxygen species (ROS) generation. In addition, the presence of CQDs helps stabilize the AgNPs, increase the effective contact surface area, and promote better nanoparticle dispersion, thereby allowing Ag^+ ions to interact more efficiently with bacterial cells. These combined effects increase oxidative stress, enhance membrane permeability, and ultimately result in efficient bacterial inactivation.[21]

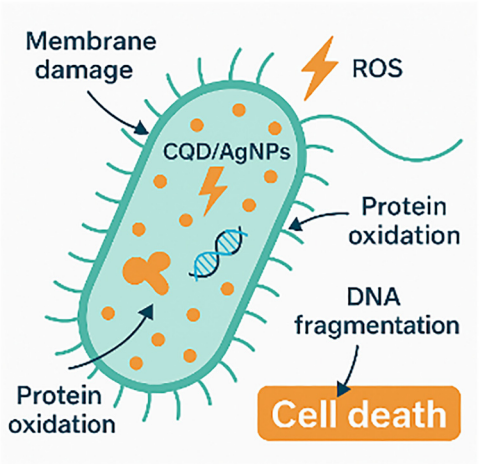

Fig. 8 The probable mechanism of the antibacterial activity of the CQD/AgNP nanocomposite.

To evaluate its potential for future biomedical applications, a preliminary cytotoxicity test was performed on the CQD/AgNPs nanocomposite using the standard MTT assay on HEK293A cells.

As shown in Fig. 9, the cells were treated with different concentrations of the nanocomposite (100, 50, 25, 12.5, and 6.25 μg mL^{-1}) for 24 h. The percentage of viable cells was

Table 4 Growth inhibition diameter value of the antibiotic plates and silver nanocomposites (M1) against ESKAPEE isolates

Test ESKAPEE	Ciprofloxacin	M1 (CQD/AgNPs)
Escherichia coli	—	15 ± 2 mm
Klebsiella pneumoniae	30 mm ± 2 mm	13 ± 2 mm
Acinetobacter baumannii	—	17 ± 2 mm
Pseudomonas aeruginosa	—	17 ± 2 mm

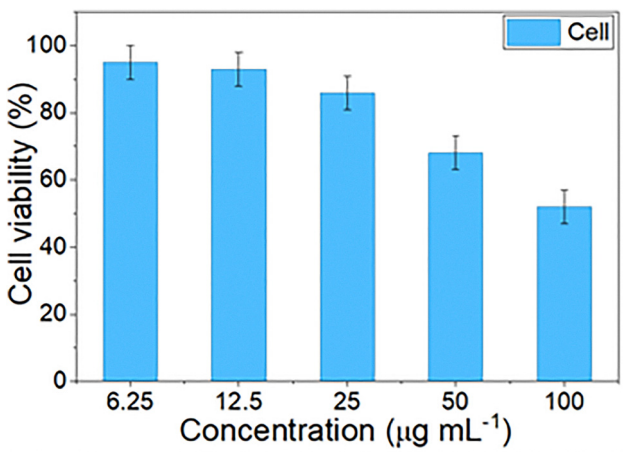

Fig. 9 Relative viability of HEK293A cells treated with different concentrations of CQD/AgNPs for 24 h.

calculated relative to the untreated control based on the absorbance of the formazan product measured at 570 nm.

The results showed a concentration-dependent reduction in cell viability; however, the viability remained above 70% at concentrations of 50 μg mL^{-1} and 25 μg mL^{-1}. This indicates that the CQD/AgNPs nanocomposite exhibits acceptable cytocompatibility at these working concentrations. These findings suggest that the material could serve as a promising candidate for the future development of antimicrobial nanomaterials or next-generation antibiotic alternatives.

Conclusion

In this study, we developed a cost-effective, green-synthesized CQD/AgNPs nanocomposite using *Psidium guajava* leaf extract, which served as both the carbon source and a natural reducing agent. The incorporated CQDs further enhanced the antibacterial performance of the composite by improving nanoparticle dispersion, stabilizing AgNPs, and contributing additional surface functional groups that promote membrane interaction and reactive oxygen species (ROS) generation.The resulting material exhibited strong antibacterial activity against multidrug-resistant (MDR) ESKAPEE pathogens, with a minimum inhibitory concentration (MIC) of 25 μg mL^{-1} against *Acinetobacter baumannii*. Structural characterization confirmed the formation of stable and uniformly dispersed nanoparticles. Importantly, the nanocomposite remained stable at room temperature for at least six months without the need for refrigeration, offering a practical advantage for storage and potential scale-up. In conclusion, these results suggest that the synthesized CQD/AgNPs nanocomposite is not only environmentally friendly and biocompatible but also a promising alternative for future antimicrobial applications.

Author contributions

Hoang Thi Thu: conceptualization; methodology; data curation; formal analysis; writing – original draft; writing – review and editing; supervision. Le Tuan Anh: resources; validation; investigation; formal analysis. Dang Thien Huong: investigation; visualization; data curation; writing – original draft. Duong Ngoc Huyen: project administration; supervision.

Conflicts of interest

The authors declare that there are no conflicts of interest to declare.

Data availability

All data supporting the findings of this study are available within the article and its supplementary information (SI). Supplementary information is available. See DOI: https://doi.org/10.1039/d5ma00802f.

Acknowledgements

The authors would like to thank the Industrial University of Ho Chi Minh City (IUH) for providing laboratory facilities and technical support for this research.

References

1 L. Daruka, M. S. Czikkely, P. Szili, Z. Farkas, D. Balogh and G. Grézal, *et al.*, ESKAPE pathogens rapidly develop resistance against antibiotics in development in vitro, *Nat. Microbiol.*, 2025, **10**(2), 313–331.
2 S. I. Ibrahim, A. M. Parambil, N. Jha, A. K. Tomar, P. Rajamani and X. Jian, *et al.*, Targeting ESKAPE pathogens with ZnS and Au@ZnS Core–Shell nanoconjugates for improved biofilm control, *Sci. Rep.*, 2025, **15**(1), 21407.
3 Md. A. Salam, Md. Y. Al-Amin, M. T. Salam, J. S. Pawar, N. Akhter and A. A. Rabaan, *et al.*, Antimicrobial Resistance: A Growing Serious Threat for Global Public Health, *Healthcare*, 2023, **11**(13), 1946.
4 Antimicrobial resistance in the EU/EEA (EARS-Net) - Annual epidemiological report for 2023.
5 A. Karnwal, A. Y. Jassim, A. A. Mohammed, A. R. M. S. Al-Tawaha, M. Selvaraj and T. Malik, Addressing the global challenge of bacterial drug resistance: insights, strategies, and future directions, *Front. Microbiol.*, 2025, **16**, 1517772.
6 M. S. Mulani, E. E. Kamble, S. N. Kumkar, M. S. Tawre and K. R. Pardesi, Emerging Strategies to Combat ESKAPE Pathogens in the Era of Antimicrobial Resistance: A Review, *Front. Microbiol.*, 2019, **10**, 539.
7 K. Rox and E. Medina, Aerosolized delivery of ESKAPE pathogens for murine pneumonia models, *Sci. Rep.*, 2024, **14**(1), 2558.
8 A. S. Rodrigues, J. G. S. Batista, M. Á. V. Rodrigues, V. C. Thipe, L. A. R. Minarini and P. S. Lopes, *et al.*, Advances in silver nanoparticles: a comprehensive review on their potential as antimicrobial agents and their mechanisms of action elucidated by proteomics, *Front. Microbiol.*, 2024, **15**, 1440065.
9 Y. Ren, Y. Zhang and X. Li, Application of AgNPs in biomedicine: An overview and current trends, *Nanotechnol. Rev.*, 2024, **13**(1), 20240030.
10 N. Al-Gburi, A. Al-Hassnawi and L. A. Al-Bayati, Biosynthesis of Silver Nanoparticles and Their Roles in the Biomedical Field: A Review, *Med. J. Babylon*, 2024, **21**(3), 493–499.
11 L. Kumar, M. Bisen, K. Harjai, S. Chhibber, S. Azizov and H. Lalhlenmawia, *et al.*, Advances in Nanotechnology for Biofilm Inhibition, *ACS Omega*, 2023, **8**(24), 21391–21409.
12 W. Chartarrayawadee, P. Charoensin, J. Saenma, T. Rin, P. Khamai and P. Nasomjai Green synthesis and stabilization of silver nanoparticles using Lysimachia foenum-graecum Hance extract and their antibacterial activity.
13 G. Kuppannan, M. Musthafa and M. Manohar, Antibacterial Activity of Wound Healing Spacer Materials Coated with Green Synthesized AgNP-AMP Conjugates against ''ESKAPE'' Members of Clinical Isolates from Different Types of Wounds, *J. Res. Med. Dent. Sci.*, 2021, **9**(4), 501.

14 A. K. Giri, B. Jena, B. Biswal, A. K. Pradhan, M. Arakha and S. Acharya, *et al.*, Green synthesis and characterization of silver nanoparticles using Eugenia roxburghii DC. extract and activity against biofilm-producing bacteria, *Sci. Rep.*, 2022, **12**(1), 8383.
15 E. O. Mikhailova, Green Silver Nanoparticles: An Antibacterial Mechanism, *Antibiotics*, 2024, **14**(1), 5.
16 Q. Ni, T. Zhu, W. Wang, D. Guo, Y. Li and T. Chen, *et al.*, Green Synthesis of Narrow-Size Silver Nanoparticles Using Ginkgo biloba Leaves: Condition Optimization, Characterization, and Antibacterial and Cytotoxic Activities, *Int. J. Mol. Sci.*, 2024, **25**(3), 1913.
17 M. A. Abdelwahab, A. Nabil, H. El-Hosainy, R. Tahway and M. S. Taha, Green synthesis of silver nanoparticles using curcumin: A comparative study of antimicrobial and antibiofilm effects on Acinetobacter baumannii against chemical conventional methods, *Results Chem.*, 2024, **7**, 101274.
18 S. Raza, M. Wdowiak, M. Grotek, W. Adamkiewicz, K. Nikiforow and P. Mente, *et al.*, Enhancing the antimicrobial activity of silver nanoparticles against ESKAPE bacteria and emerging fungal pathogens by using tea extracts, *Nanoscale Adv.*, 2023, **5**(21), 5786–5798.
19 S. El Ghacham, L. Hejji, Y. Aoulad El Hadj Ali, A. Wahby, L. Tamegart and L. Pérez-Villarejo, *et al.*, Enhanced antibacterial and wound healing efficacy of a novel CQDs@AgNPs@CS-based nanocomposites: A multifunctional approach for advanced wound care, *Int. J. Biol. Macromol.*, 2025, **311**, 143621.
20 T. Liu, Q. Pang, K. Mai, X. He, L. Xu and F. Zhou, *et al.*, Silver nanoparticle@carbon quantum dot composite as an antibacterial agent, *RSC Adv.*, 2022, **12**(16), 9621–9627.
21 S. El Ghacham, L. Hejji, Y. Aoulad El Hadj Ali, A. Azzouz, L. Pérez-Villarejo and L. Tamegart, *et al.*, Green-synthesized carbon quantum dots–silver nanocomposites for broad-spectrum antimicrobial and wound healing applications, *J. Drug Delivery Sci. Technol.*, 2025, **108**, 106964.
22 J. Jia, Y. Sun, Y. Zhang, Q. Liu, J. Cao and G. Huang, *et al.*, Facile and Efficient Fabrication of Bandgap Tunable Carbon Quantum Dots Derived From Anthracite and Their Photoluminescence Properties, *Front. Chem.*, 2020, **8**, 123.
23 S. Sheshmani, M. Mardali, S. Shokrollahzadeh, Y. Bide and R. Tarlani, Synthesis, optical, and photocatalytic properties of cellulose-derived carbon quantum dots, *Sci. Rep.*, 2025, **15**(1), 19027.
24 M. Kumar, S. Chinnathambi, N. Bakhori, N. Abu, F. Etezadi and V. Thangavel, *et al.*, Biomass-derived carbon dots as fluorescent quantum probes to visualize and modulate inflammation, *Sci. Rep.*, 2024, **14**(1), 12665.
25 E. E. Ateia, O. Rabie and A. T. Mohamed, Assessment of the correlation between optical properties and CQD preparation approaches, *Eur. Phys. J. Plus*, 2024, **139**(1), 24.
26 R. Kaur, J. Singh, D. Kathuria and A. S. Matharu, Waste biomass-derived CQDs and Ag-CQDs as a sensing platform for Hg2+ ions, *Sustainable Chem. Pharm.*, 2022, **29**, 100813.
27 P. K. Praseetha, R. I. J. Litany, H. M. Alharbi, A. A. Khojah, S. Akash and M. Bourhia, *et al.*, Green synthesis of highly fluorescent carbon quantum dots from almond resin for advanced theranostics in biomedical applications., *Sci. Rep.*, 2024, **14**(1), 24435.
28 A. Amirsoleimani, Z. Bahrami, H. Abdoos and K. Kafshdouzan, Synthesis and characterization of Zn-doped carbon dots derived from calendula officinalis and glucose: Antibacterial and photoluminescence properties, *Carbon Trends*, 2025, **20**, 100537.
29 M. Ghirardello, J. Ramos-Soriano and M. C. Galan, Carbon Dots as an Emergent Class of Sustainable Antifungal Agents, *ACS Nano*, 2025, **27**, 24377–24403.
30 E. A. Diab, M. Ghali and M. M. Mosaad, *In vitro* antimicrobial and anticancer potentials of green synthesized luminescent carbon quantum dots derived from artichoke leaves, *Sci. Rep.*, 2025, **15**(1), 16199.
31 A. Saravanan, P. Das, M. Maruthapandi, S. Aryal, S. Michaeli and Y. Mastai, *et al.*, Heteroatom co-doping (N, NS, NB) on carbon dots and their antibacterial and antioxidant properties, *Surf. Interfaces*, 2024, **46**, 103857.
32 A. Saravanan, M. Maruthapandi, P. Das, S. Ganguly, S. Margel and J. H. T. Luong, *et al.*, Applications of N-Doped Carbon Dots as Antimicrobial Agents, Antibiotic Carriers, and Selective Fluorescent Probes for Nitro Explosives, *ACS Appl. Bio Mater.*, 2020, **3**(11), 8023–8031.
33 M. A. Zarouki, L. Tamegart, L. Hejji, Y. A. El Hadj Ali, A. E. Ayadi and L. P. Villarejo, *et al.*, Graphene quantum dots based on cannabis seeds for efficient wound healing in a mouse incisional wound model: Link with stress and neurobehavioral effect, *Int. J. Pharm.*, 2024, **649**, 123658.
34 J. Peng, W. Gao, B. Gupta, Z. Liu, R. Romero Aburto and L. Ge, *et al.*, Graphene Quantum Dots Derived from Carbon Fibers, *Nano Lett.*, 2012, **12**, 844–849.
35 F. Shen, Z. Lu, K. Yan, K. Luo, S. Pei and P. Xiang, Synthesis and properties of carbon quantum dots as an antimicrobial agent and detection of ciprofloxacin, *Sci. Rep.*, 2025, **15**(1), 28535.
36 Z. Li, L. Deng, I. A. Kinloch and R. J. Young, Raman spectroscopy of carbon materials and their composites: Graphene, nanotubes and fibres, *Prog. Mater. Sci.*, 2023, **135**, 101089.
37 Y. Dong, Q. Wang, L. Wan, X. You and Y. Chi, Carbon based dot capped silver nanoparticles for efficient surface-enhanced Raman scattering, *J. Mater. Chem. C*, 2016, **4**(31), 7472–7477.
38 B. I. Salman, Synthesis of highly fluorescent green carbon quantum dots from Prunus armeniaca for the determination of lisinopril in human plasma, *Sci. Rep.*, 2025, **15**(1), 32502.
39 C. D. Doern, When Does 2 Plus 2 Equal 5? A Review of Antimicrobial Synergy Testing, *J. Clin. Microbiol.*, 2014, **52**(12), 4124–4128Carroll KC, editor.
40 D. Gautam, K. G. Dolma, B. Khandelwal, M. Gupta, M. Singh and T. Mahboob, *et al.*, Green synthesis of silver nanoparticles using *Ocimum sanctum* Linn. and its antibacterial activity against multidrug resistant *Acinetobacter baumannii*, *PeerJ*, 2023, **11**, e15590.
41 F. Kakian, N. Arasteh, E. Mirzaei and M. Motamedifar, Study of MIC of silver and zinc oxide nanoparticles, strong and cost-effective antibacterial against biofilm-producing

Acinetobacter baumannii in Shiraz, Southwest of Iran, *BMC Infect. Dis.*, 2024, **24**(1), 593.

42 M. S. Ahmed, F. A. Abdulrahman Zirak and Z. M. A. Taha, The effect of silver nanoparticles on the antimicrobial activity of cloned nisin against extensively drug-resistant Acinetobacter baumannii'', *J. Infect. Public Health*, 2024, **17**(9), 102501.

43 S. Shamsoddini, M. Davoudi, S. Shahbazi and S. Zare Karizi, Green synthesis of silver nanoparticles using Acroptilon repens aqueous extract and their antibacterial efficacy against multidrug-resistant Acinetobacter baumannii, *Mol. Biol. Rep.*, 2024, **52**(1), 47.

44 N. D. Nogbou, D. R. Mabela, B. Matseke, N. S. Mapfumari, M. E. Mothibe and L. C. Obi, *et al.*, Antibacterial Activities of Monsonia Angustifolia and Momordica Balsamina Linn Extracts against Carbapenem-Resistant Acinetobacter Baumannii, *Plants*, 2022, **11**(18), 2374.